frontiers in Electronics

ORIGINAL RESEARCH
published: 25 March 2022
doi: 10.3389/felec.2022.848618

Multiplexing Error and Noise Reduction in Electrical Impedance Tomography Imaging

*Martina Barreiro[1], Pablo Sánchez[1], Julián Vera[1], Matías Viera[1], Isabel Morales[1], Antonio Hector Dell´Osa[2], Pedro Bertemes-Filho[3] and Franco Simini[1]**

[1]*Núcleo de Ingeniería Biomédica de las Facultades de Medicina e Ingeniería, Universidad de la República, Montevideo, Uruguay,* [2]*Laboratorio de Electrónica Aplicada y Biomedicina, Instituto de Desarrollo Económico e Innovación, Universidad Nacional de Tierra del Fuego, Ushuaia, Argentina,* [3]*Department of Electrical Engineering, Universidade do Estado de Santa Catarina, Joinville, Brazil*

Electrical Impedance Tomography design can be simplified to obtain a low cost 16 electrodes edema monitoring clinical instrument by using voltage measurement multiplexing. Multiplexers introduce errors, which we have estimated by consecutive phantom measurements both using voltage multiplexers and by selecting the electrodes by hand, all other things being the same. Noise is taken care of by averaging. The EIDORS reconstruction of the phantom with multiplexed measurements is compared to the hand-selected electrode measurements reconstruction. The difference image obtained is considered an estimation of the multiplexer induced error. This measurement error is subtracted from the multiplexed object measurement matrix, giving a modified reconstruction which is closer to the hand-selected electrodes measurement based reconstruction than the multiplexed reconstruction. The quality factor of the uncorrected multiplexer obtained image of 57% is increased to 83% which is the best increase of three methods described. This suggests the benefit of a "calibration" phase for all 16 electrodes, prior to EIT reconstruction, using a set-up-specific "error matrix" to correct the data matrix before submission to the reconstruction method.

Keywords: EIT, phantom, multiplexer, noise reduction, EIDORS, error reduction

OPEN ACCESS

Edited by:
Jie Zhao,
Fudan University, China

Reviewed by:
Yu Wu,
University College London, United Kingdom
Soon-Jae Kweon,
New York University Abu Dhabi, United Arab Emirates

****Correspondence:***
Franco Simini
simini@fing.edu.uy

Specialty section:
This article was submitted to Bioelectronics, a section of the journal Frontiers in Electronics

Received: *04 January 2022*
Accepted: *01 March 2022*
Published: *25 March 2022*

Citation:
Barreiro M, Sánchez P, Vera J, Viera M, Morales I, Dell'Osa AH, Bertemes-Filho P and Simini F (2022) Multiplexing Error and Noise Reduction in Electrical Impedance Tomography Imaging. Front. Electron. 3:848618. doi: 10.3389/felec.2022.848618

INTRODUCTION

Electrical impedance tomography (EIT) is based on multiple determinations of electrical bioimpedance on the outer boundaries of a section of the human body (Jongschaap et al., 1994). The technique consists of applying a sinusoidal current signal to a pair of electrodes and measuring the resulting voltage potentials of all other pairs and repeating for all injection pairs of the boundary. A current signal (high frequency, low intensity) is applied, and the voltages are measured, or vice versa, depending on the application (Bertemes-Filho, 2021; Mohamadou et al., 2012). With these two parameters, by means of Ohm's law, the resulting impedance can be calculated. In biomedical applications, the technique obtains the electrical bioimpedance of a transverse region of the patient, defined by placing the electrodes around it. This process results in border restrictions, which will be used to solve the so-called inverse problem (Calderón, 1980; Grimnes and Ørjan, 2015). Since different tissues have different impedances, it is possible to characterize them from the bioimpedance measurements, thus achieving a tomographic image of the region (Valentinuzzi et al., 1996).

EIT presents many advantages, such as the ability to generate a tomographic image of a region without causing damage to the patient, due to high-frequency, low-intensity currents that stay well below perception thresholds (Brown, 2009; IEC, 2016; IEC, 2020). However, it presents an important disadvantage in resolution compared to ionizing radiation image acquisition. This is partially a consequence of the finite quantity of data at the region's border, which in turn depends on the number of electrodes used. Nonetheless, increasing the number of electrodes does not guarantee a significant improvement in resolution, as seen in Adler & Lionheart (2006); Simini et al. (2018) and is also often impractical. EIT systems typically use 8 to 32 electrodes for measurements (Grimnes and Ørjan, 2015; Swisstom, 2015; Dräger AG, 2020; Harris et al., 2020; Adler and Holder, 2021). EIT reconstruction has lately become popular after the publication of several guidelines to design specific tomographic applications, such as the EIT-kit (Zhu., et al., 2021).

IMPETOM-Clínico is a 16-electrode bioimpedance measurement device developed in our laboratory, to obtain tomographic images of the transverse section of a patient or a phantom, in real time. The distinctive characteristic of IMPETOM is that no anatomical precision is pursued, but quantitative water occupation in the lungs is pursued instead (Simini et al., 2018). Due to the number of electrodes which would require several electronic circuits, the concept of multiplexing arises naturally to reduce the number of current generation as well as acquisition/processing channels (Wu et al., 2021).

The present article compares two ways of data acquisition, in a practical way, for EIT reconstruction: 1) hand-selected electrodes measurements and 2) multiplexed measurements. Multiplexing is applied to both current injection and voltage measurement.

The first measurement consists of manually selecting the electrodes used to inject current and to measure voltage. The second way uses multiplexers, which automatize the selection of injection and measurement electrodes, by enabling channels via an Arduino-based program. The differences between these two will be studied in detail in this article to check the relevance of the electronic noise added by the multiplexers and to suggest a way to offset it.

OBJECTIVE

The objective of the present research was to quantify the error introduced by multiplexers in the measurements of EIT voltages (and to the resulting images) in a saline-filled phantom and in the same phantom with a low-conductivity object. The multiplexer-induced error is used to show a corrected EIT image of the low-conductivity object phantom.

METHODS

Electrical Bioimpedance Measurements

We have taken voltage measurements from adjacent electrodes of a plastic phantom with 16 steel electrodes all around it, following the adjacent method procedure (Grimnes and Ørjan, 2015). The injection current of 1 mA amplitude and frequency of 30 kHz were applied in a series of 16 pairs of contacts, the selection of electrodes being either by hand or using the injection multiplexer circuit. Voltages were also taken either selecting the electrode pairs manually or using the voltage measurement multiplexer circuit. Hand-selected electrodes measurements consist of the same measurement of the EIT system but with the multiplexers omitted; the selection of the injection pair and the measured pair of electrodes was performed using hand using alligator clips. It should be emphasized that stray capacitance from cables and the electronic circuit itself will be acting in both types of channel selection. Therefore, only the stray impedance of the multiplexer was the difference between the two measurements and thus enabled the calculation of the error. Both multiplexer circuits, namely, current and voltage multiplexers will be addressed in this article. The voltage measurements were organized in similar matrices.

The measurements were taken on both a saline-filled phantom and a phantom filled with saline with a low-conductivity object inside. The saline measurements simulated a "non-signal" situation, i.e., an estimation of noise of the method, while the low-conductivity object measurements are the "signal" situation. **Figure 1** shows the phantom filled with saline and filled with saline containing a low-conductivity object.

The measurements taken are organized in matrices according to the following:

ZM: saline-filled phantom with hand-selected electrodes measurements.

AM: low-conductivity object in saline phantom with hand-selected electrodes measurements.

ZX: saline-filled phantom with multiplexers for current injection and voltage measurements.

AX: low-conductivity object in the saline-filled phantom with multiplexers for current injection and voltage measurements.

Instrumentation Used

Electrical bioimpedance was evaluated using the following instruments:

1) Siglent ® SHS820 handheld digital oscilloscope.
2) Tektronix ® PS280 DC power supply.
3) Extech ® EX505 multimeter.
4) Fluke ® 73 multimeter.
5) IMPETOM-Clínico: an EIT system under development.

IMPETOM-Clínico is the latest version of an EIT device designed and built in our laboratory, and IMPETOM ® (Simini et al., 2018) is based on several partial designs (Ferreira et al., 2002; Hartman et al., 2002; González et al., 2005; Quinteros et al., 2007; Santos, 2014; Alfaro et al., 2015).

Our present version consists of three main blocks (**Figure 2**): 1) signal generation, 2) multiplexers, and 3) analog signal processing. The first block generates the alternating 30 kHz current to be injected into the phantom, using DDS technology (Analog Devices Inc, 1999) and appropriate filtering. The DDS used is AD9833, which is a low-power,

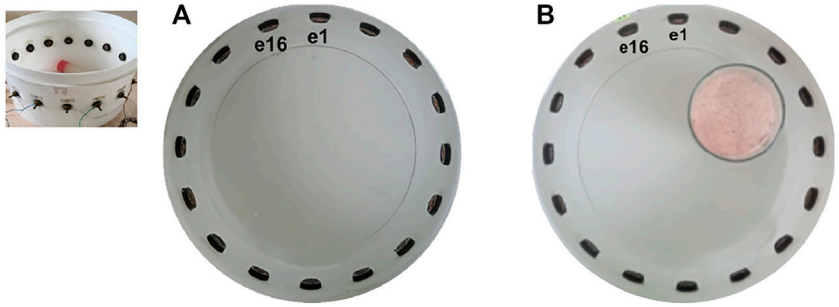

FIGURE 1 | Phantom with steel electrodes *e1* through *e16* in clockwise direction from above: **(A)** filled with saline solution and **(B)** filled with saline solution and containing a low conductivity object (a glass filled with sand, between *e3* & *e4*). Inset: general view of the phantom, with 23 cm diameter.

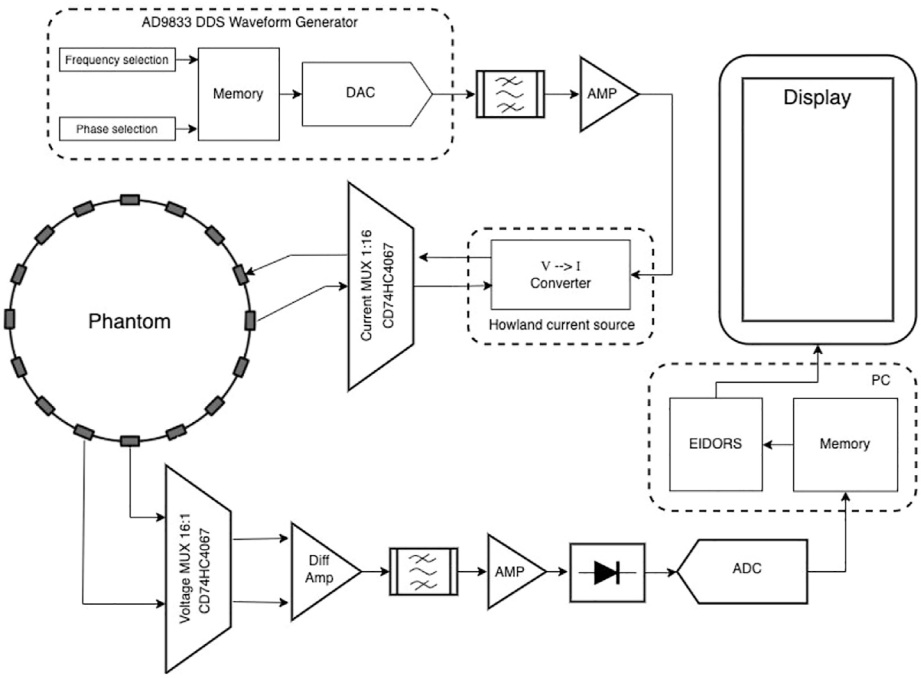

FIGURE 2 | Block diagram of IMPETOM-Clínico. In order to evaluate the effects of multiplexers, they are omitted to obtain impedance values (and resulting reconstructed images) which are then compared to the images obtained with the complete circuit. DDS used is AD9833; MC33077 is the operational amplifier that we used for the Howland current source, both band-pass filters include 30 kHz, but the band-pass filter prior to the measurement has a quality factor of Q = 37.

programmable waveform generator capable of producing sine, square, and triangular waveforms. The frequency and phase of the output signal are programmable. After the DDS, there is an active band-pass filter with 1.6–371 kHz bandwidth that is used to smooth the digital signal prior to injection into the phantom to remove DC components and switching noise above 1 decade over the frequency of interest, 30 kHz. The 1 mA current is given by an internal resistor of the Howland current source.

The multiplexers block is in charge of multiplexing the 16 channels. It consists of two pairs of 16:1-channel analog multiplexer/demultiplexers, one for current injection and the other for voltage measurements. We used CD74HC4067 analog multiplexer/demultiplexer (Texas Instrument Inc., 2003), which features a low "on"-resistance (typically Ron≈70 Ω), connected in series between the multiplexer's input and output pins. Other multiplexer/demultiplexer ICs have been discarded due to their higher "on"-resistance such as CD4051. The electronic properties of the signal circuit are those of CMOS transistors with low resistance during saturation. Each multiplexer is controlled by four pins, and it is powered by the 5 V supply of Arduino ®. The circuit schematic of the multiplexer stage is shown in **Figure 4**.

Multiplexers introduce error due to their internal parasitic capacitance, leakage current, and suboptimal circuit elements, in addition to the random noise of the "on"-resistance of the CMOS transistors. A typical CMOS switch circuit can be found in the

manufacturer´s tutorial documentation (Analog Devices Inc, 2009). The result of introducing multiplexers in the signal acquisition path, both in the current injection portion and in the voltage measurement, has an inevitable effect on the resulting EIT image.

The analog signal processing block also receives the voltage measurement coming from the multiplexer stage and performs filtering, amplification, and DC conversion for digitalization, which is performed by a half-wave voltage rectifier in conjunction with a voltage divider. This allows rectifying the input signal and to size it within the range of admissible values for the microcontroller. After that, the signal is acquired by the ADC converter of Arduino ® with 10-bit resolution. The data acquired are voltage values which can be accurately measured only if the band-pass filter at 30 kHz has a high quality factor; we have implemented one with Q = 37. In order to get those values, we assume resistance measurements between each pair of electrodes, neglecting any imaginary part.

The oscilloscope SHS820 has been occasionally calibrated as usual in a university teaching laboratory according to the manufacturer's instructions.

EIT Phantom

To test the EIT system under development, IMPETOM-Clínico, a cylindrical plastic phantom, was built with 23 cm diameter and 15 cm height, with a capacity of 5 L. We placed 16 steel electrodes on the cylindrical surface, 8 cm from the bottom, drawing a complete circumference. The electrodes are submerged in saline inside the phantom and crossed to the outside where contacts allow easy connections to circuitry. **Figure 1** shows the phantom developed.

Saline was prepared by adding sodium chloride (NaCl) to water at an ambient temperature (0.9 g of salt per liter) which corresponds to 190 mS/m of conductivity (Kao et al., 2008).

Measurement Protocol

1) The 5-L phantom is filled with 3.5 L of saline water. The electrodes are 1 cm below the level of saline.
2) Electrode connections were made as shown in **Figure 3**: the current generator to the first pair and voltage acquisition to the first adjacent pair, then to the next pair, and so on, until the last pair.
3) Hand-selected electrodes measurements of voltage at 13 successive pairs of electrodes for every pair of electrodes used to inject current, on the objectless phantom. For each one of the 16 pairs of electrodes, 13 voltage measurements are taken, i.e., 208 values. We used four alligator clips, two to connect the current source to two adjacent phantom electrodes and two to measure voltage in successive electrode pairs. It took 1 hour for two authors to obtain this set of values. Matrix ZM is filled in with these values by Arduino ® software.
4) A low-conductivity cylindrical object is introduced resting on the bottom of the phantom and filled with sand up to 1 cm above the water level. The center of the object rests in the middle of the radius of the phantom between electrodes 3 and 4.

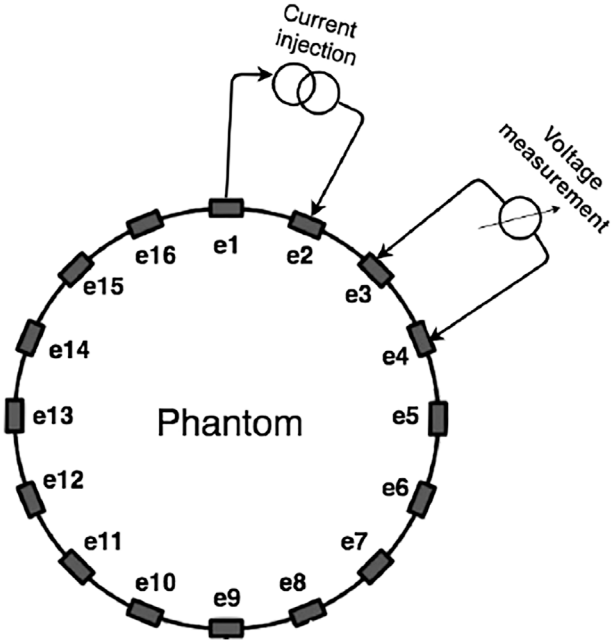

FIGURE 3 | Connections made for hand-selected electrodes measurements.

5) Hand-selected electrodes measurements of the low-conductivity object give a new set of 208 voltage values. Matrix AM is filled in with these values. It also took 1 hour to obtain these values.
6) Connections are made as shown in **Figure 4**: the current generator to current multiplexer circuit, voltage acquisition circuit to multiplexer circuit, and 16 electrodes to multiplexers. See **Figure 4**, in which V- and V+ are the voltages at each electrode pair.
7) Multiplexed measurements starting with the same pairs of electrodes as in the hand-selected case of the phantom with the low-conductivity object. The integrated circuit CD74HC4067 was used to connect each electrode to a multiplexer channel. Two multiplexers select which electrode pair has to be voltage-measured while two other multiplexers select the electrode pair to which the current is to be injected into. A software program commands the selector bits to operate both the injection and resulting voltage measurements. Matrix AX is filled in with these values by the Arduino ® software.
8) Removal of the low-conductivity cylindrical object from within the phantom.
9) Multiplexed measurements, starting with the same pairs of electrodes as in the hand-selected case, of the saline only-filled phantom. Matrix ZX is filled in with these values.

Multiplexer-Induced Error Estimation

The error is characterized in the absence of the low-conductivity object. The corrections can then be applied once the low-conductivity object has been placed in the phantom.

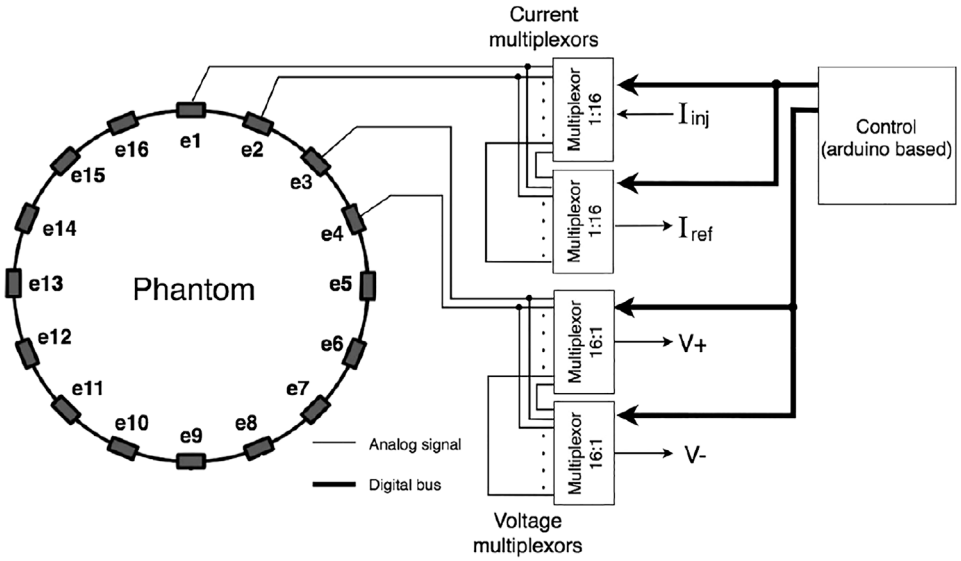

FIGURE 4 | Basic electrical bioimpedance measurement connections with multiplexed injection current and multiplexed voltage measurements. Adapted from Simini (Simini et al., 2018).

The error introduced by the multiplexers was defined and estimated by three methods:

1) Matrix element by matrix element difference in voltage measurements of the hand-selected electrodes recorded values subtracted from the multiplexer set of values in the absence of a low-conductivity object. ZX-ZM, ideally this subtraction matrix should be null.
2) Mean value of differences of the matrix elements that share the same current injection electrodes in the saline phantom. The error is estimated for each column of the matrix: let f_c(ZX-ZM) be the result of the subtraction of the average of the column from each element.
3) Mean value of differences of the matrix elements that share the same voltage measurement electrodes. The error is estimated for each row of the matrix: let f_r(ZX-ZM) be the result of the subtraction of the average of the row from each element.

Quality Factor of Tomographic Image Reconstruction

We suggest adopting a quality factor to represent the improvement of EIT reconstruction images and thus to compare the three correction methods. This quality factor (QF) is defined in **Eq. 1**.

$$QF = 10\left(10 - \sqrt{\sum_{i=1}^{N}\sum_{j=1}^{M}\left(A_{ij} - B_{ij}\right)^2}\right), \quad (1)$$

where A_{ij} represents the measurement matrix elements at row i and column j of AM, and B_{ij} represents the measurement matrix elements post correction. QF was calculated for each correction method, to compare them to the hand-selected electrodes measurements taken as the gold standard.

EIT Reconstruction

EIT reconstruction was performed using the EIDORS system (Valentinuzzi et al., 1996; Adler and Lionheart, 2006) with matrices ZM, AM, AX, and ZX, as shown in **Figure 5** (ZM, AM) and **Figure 6** (AX, ZX). We considered ZX-ZM as an error estimation matrix. AM would be the correct EIT image obtained as a partially degraded image AX, due to the multiplexers.

To better evaluate the effect of multiplexing on EIT image reconstruction, the hand selection method was compared to the multiplexed one by using the same setup for both of them, namely current magnitude, electrode sequence, signal amplification/acquisition, and image reconstruction method. **Figure 7** shows the representation of the 208 voltage measurements in both methods. Identification of **Figure 7A** with **Figure 7B** would be expected in case multiplexing was neutral to EIT reconstruction, especially because every single voltage is the result of averaging 100 measurements.

Multiplexer-Induced Error Correction

Since we consider (ZX-ZM) as the error introduced by the multiplexers, we use it to correct all subsequent images obtained with multiplexers. The error estimation methods are described in Section 3.5, i.e., the image difference for saline is subtracted from the object reconstruction. **Figures 8–11** compare the different results of correcting with the three error estimation methods. **Figure 8** shows hand-selected electrodes measurements of the saline-filled phantom and the same phantom with a low conductivity object. **Figure 9** is the result of element-by-element subtraction of the two matrices (first method); **Figure 10** is the result of column-wise average subtracted from elements (second method), and **Figure 11** is the line-wise average subtracted from all elements (third method).

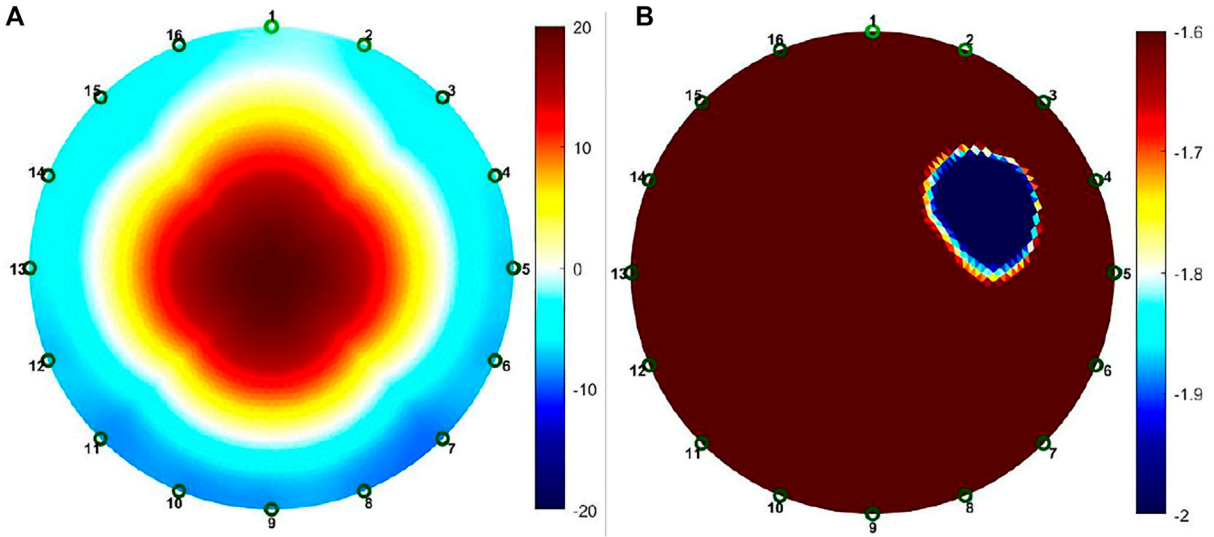

FIGURE 5 | EIT reconstruction performed using data acquired by hand selection of electrodes. **(A)** ZM: saline-filled phantom and **(B)** AM: saline-filled phantom containing a low-conductivity cylinder between electrodes 3 & 4, reconstructed using EIDORS. Scales vary for the purpose of generating better image representation.

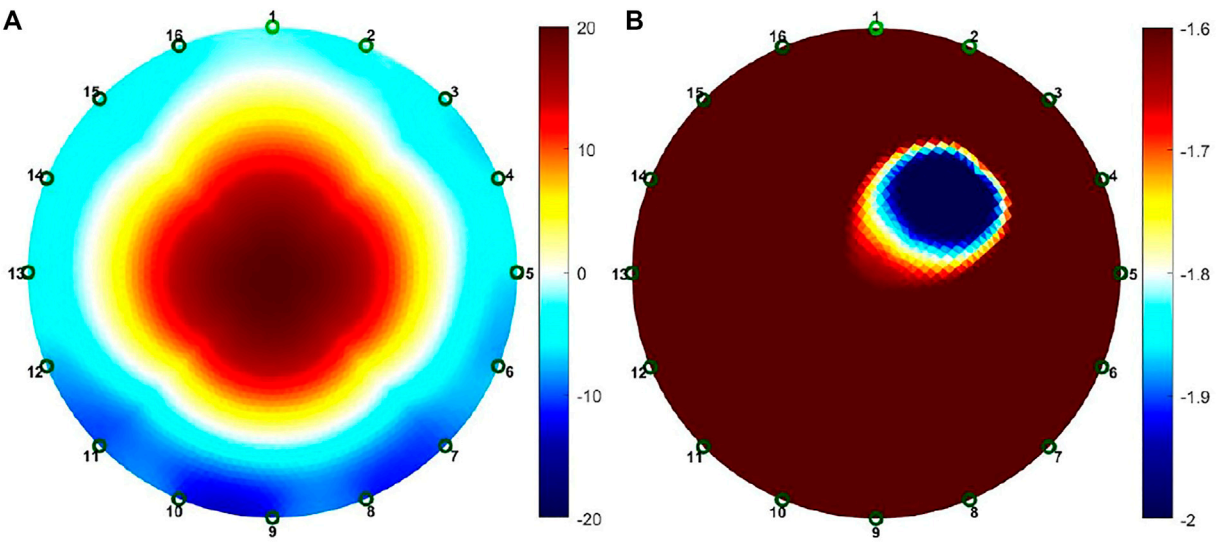

FIGURE 6 | EIT reconstruction performed using data acquired via multiplexers. **(A)** ZX: saline-filled phantom and **(B)** AX: saline-filled phantom containing a low-conductivity cylinder between electrodes 3 & 4, reconstructed using EIDORS. Scales vary for the purpose of generating better image representation.

RESULTS

The hand-selected and multiplexed EIT images for the saline phantom and phantom with a low-conductivity object are shown in **Figures 5**, **6**. The estimation of the error as element-by-element "difference image" was calculated as shown in (**Figures 6A**, **7A**) which is ZX-ZM and is shown in **Figure 12A**.

The EIT error-corrected reconstruction images differ depending on which of the three methods is used to correct the multiplexer-induced error, as shown in **Figures 9**–**11**.

The image difference (AX-f(ZX-ZM)-AM) helps to better evaluate the low-conductivity cylinder reconstruction, according to the three methods, in which f is element-by-element subtraction for the first method, f_c for column-wise, and f_r for line-wise subtraction. They should be better than the AX image because AX includes the multiplexer error, as shown in **Figures 12A,B** as well as **Figures 13A,B**.

The error is characterized numerically by QF. The results are shown in **Table 1**, in which QF values are given for each method, with the lowest error for method 1, which turns out to be the best of the three.

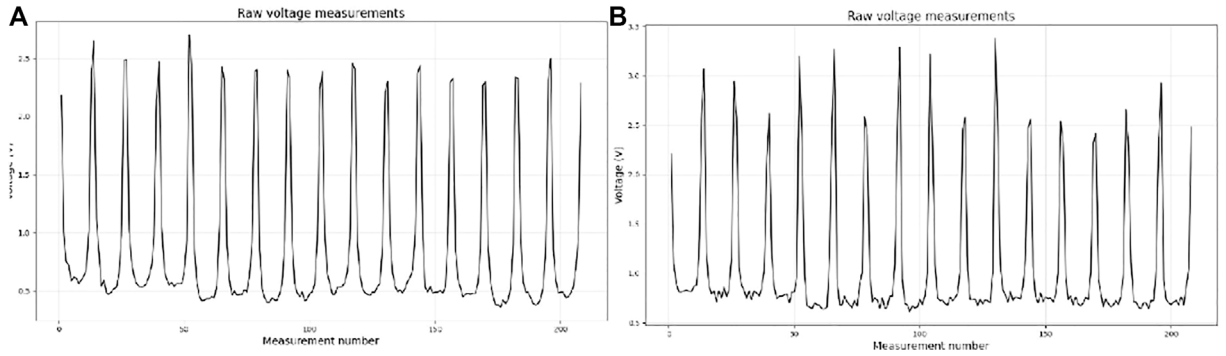

FIGURE 7 | Saline-filled phantom raw voltages, showing typical "U" shapes. **(A)** Data acquired by hand selection of electrodes. **(B)** Data acquired via multiplexers.

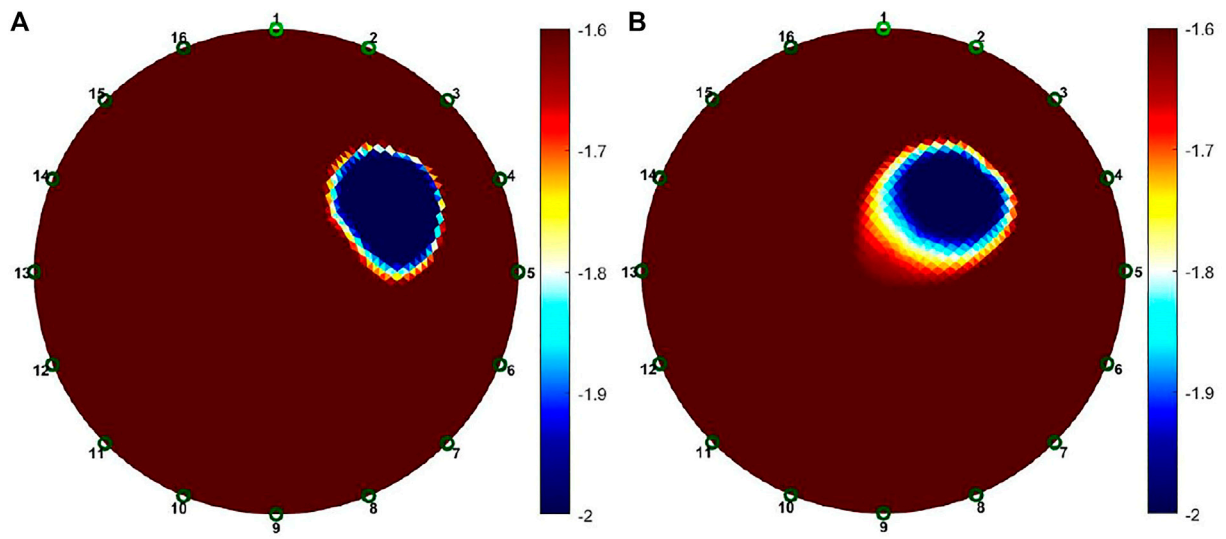

FIGURE 8 | Reconstruction of the saline-filled phantom using data obtained by **(A)** AM (hand selection) and **(B)** *AX* (multiplexed with no correction). Additional noise is observed in **(B)**. QF = 57.

We see at first glance a great similarity between **Figures 8A,B**. This is now confirmed by **Figure 13** and **Table 1**, in which the QF of **Figure 9** (first method) is the best.

Method 2 and method 3 are similar. Despite the fact that they both represent an improvement from the original multiplexed data QF = 57, their performance with QF = 67 is less than method 1 with QF = 83. However, method 1 needs more computing power to be executed because the subtraction involves two full matrices instead of matrices with rows (or columns) with the same value. So, it has a disadvantage in comparison with the other two methods considered.

We can derive from these results that applying an element–element correction, which takes into account the error introduced by multiplexers to the homogenous phantom data, may be a contribution to attenuate multiplexer electric noise in EIT circuits.

DISCUSSION

In this article, we have revisited the IMPETOM design to produce a prototype which would be transferable to an industrial company for commercialization. In doing so, a new design of the current injection and voltage measurement was necessary. To evaluate the effect of multiplexing, both for current input and voltage output, we have compared the resulting images using simple hand-selected electrodes measurements data with images obtained with our full circuit including multiplexers.

The laboratory instrumentation used, as described in **Section 3.2**, was adequate for the goals we set to ourselves. We used a handheld digital oscilloscope, Siglent SHS820, with good accuracy. Although a good digital multimeter could have performed the job, the oscilloscope gave us the additional

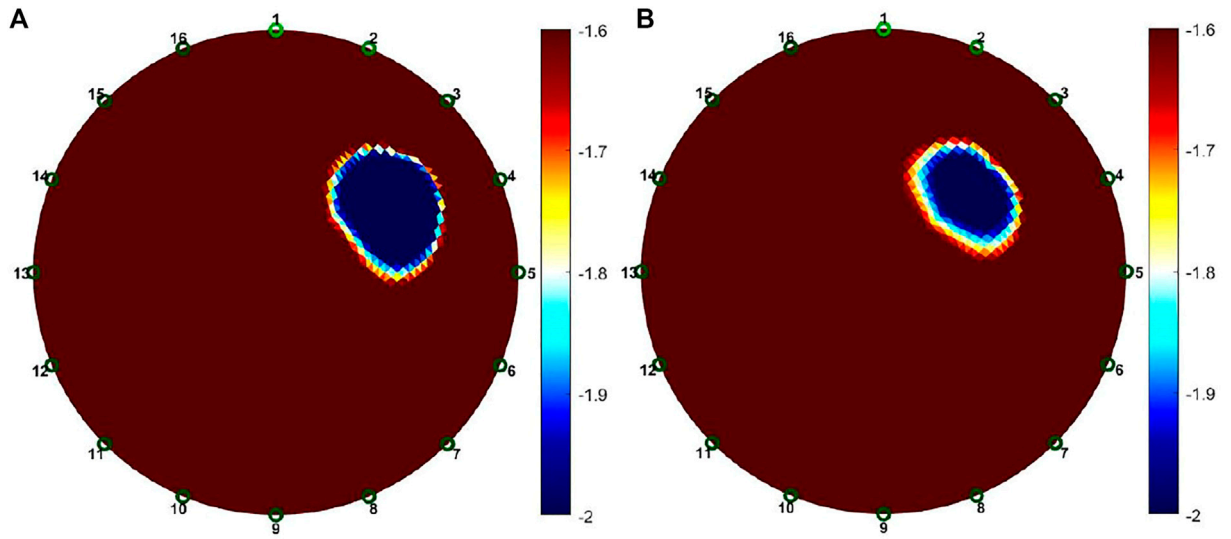

FIGURE 9 | Reconstruction of the saline-filled phantom using data obtained by **(A)** AM (hand selection) and **(B)** AX (multiplexed corrected using the first method). QF = 83.

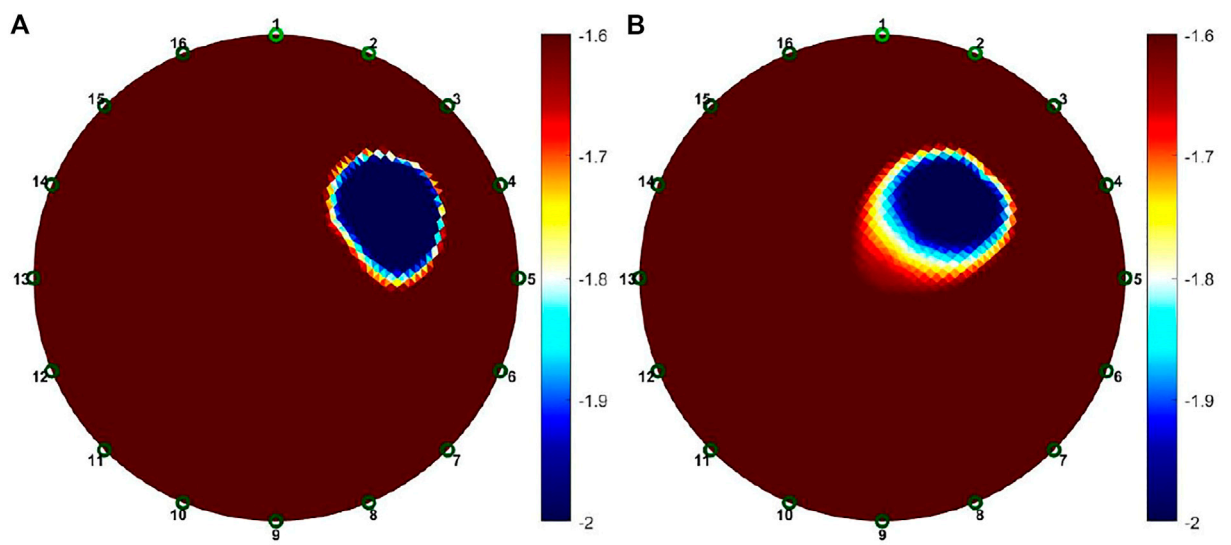

FIGURE 10 | Reconstruction of the saline-filled phantom using data obtained by **(A)** *AM* (hand selection) and **(B)** *AX* (multiplexed corrected using the second method). QF = 67.

information of the stable signal at all times prior to determining the root mean square value (RMS) of signals.

Rather than estimating the effect of multiplexer circuits at the single signal level, we have compared the overall result of image reconstruction which is ultimately the goal of EIT. The gold standard or reference image is the one we have obtained without multiplexers, i.e., hand selecting every signal at each one of the 16 electrodes of the phantom. This approach has the advantage of encapsulating all possible errors associated with multiplexers into one situation. The disadvantage is that it includes the time-consuming procedure we have followed in our protocol.

Comparing images may be a very subjective task, and this is the reason why we have suggested an overall quality factor for the images with respect to the gold standard. Considering that the gold standard (no multiplexer error) has QF = 100%, without correction, the QF of the phantom image with a low-conductivity solid was measured as 57%. We have tested three error reduction methods to compensate for the multiplexer-introduced error. The three methods foresee calibration situations with the saline-filled

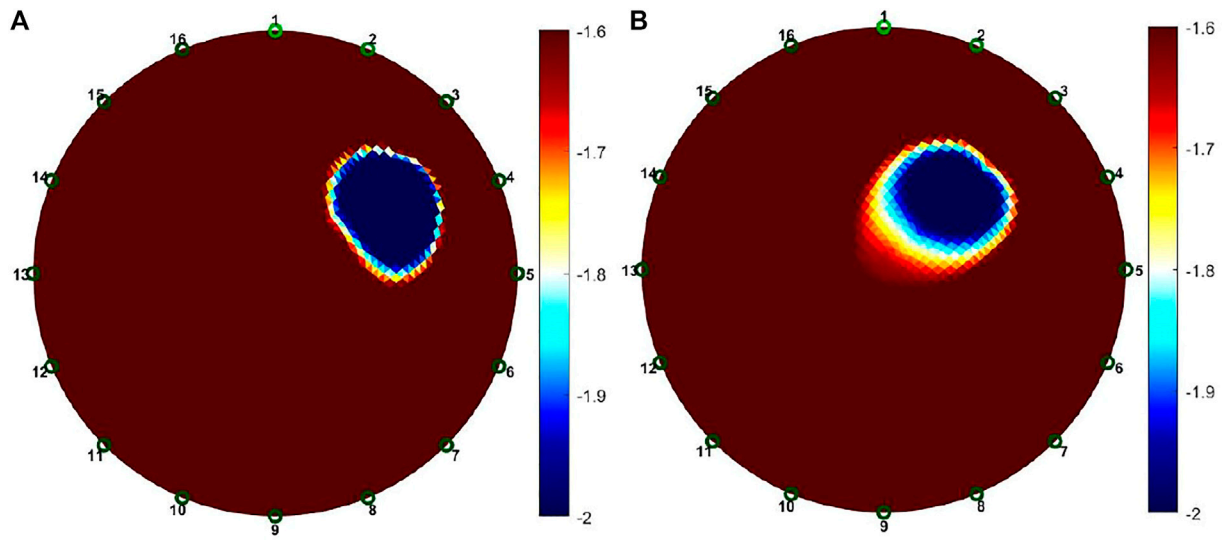

FIGURE 11 | Reconstruction of the saline-filled phantom using data obtained by **(A)** AM (hand selection) and **(B)** *AX* (multiplexed corrected using the third method). QF = 67.

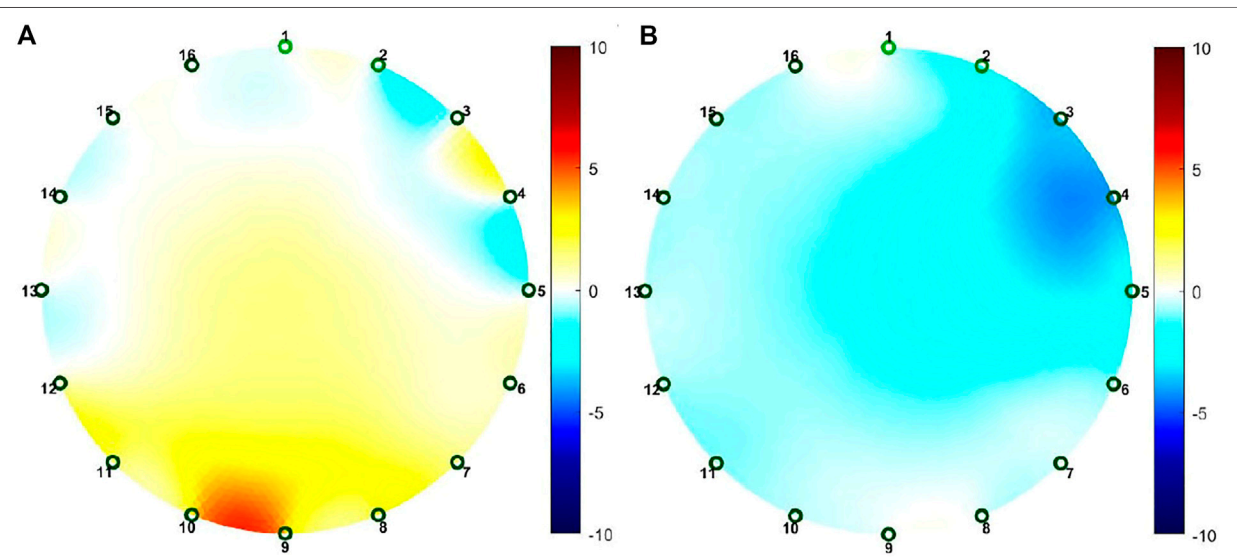

FIGURE 12 | (A) Error image (ZX-ZM) as a graphical estimation of the error introduced by the multiplexers. **(B)** Error Image AX-(ZX-ZM)-AM obtained by element-by-element subtraction to correct the multiplexed image.

phantom. The hand-selected electrodes measurement of the saline-filled phantom turned out to be different from the same phantom measured using multiplexers, which confirmed that multiplexers introduce some noise. The difference between the two images is considered our basic error image. The first method consists of subtracting, element by element, the difference matrix of the multiplexer from the hand-selected one. A good increase in the QF is observed when we apply the correction to the low-conductivity object image obtained with multiplexers. Subjectively, the image of **Figure 9B** is more similar to that of **Figure 9A** than **Figure 8B**. Correction method 1 increased the QF from 57% to 83%. This QF is closer to 100% than the ones obtained by the other two methods.

In an attempt to average multiplexer noise column-wise or line-wise in the voltage data matrix obtained, we have defined method 2 and method 3 as the subtraction of the multiplexer matrix minus the row or column mean value of each element. Interestingly, both methods have identical numerical results in which they only increase QF from 57% to 67%.

The results of this work allow us to proceed in the design of IMPETOM-Clínico, provided we can include a calibration instance in the device. Hand-selected data for phantoms and,

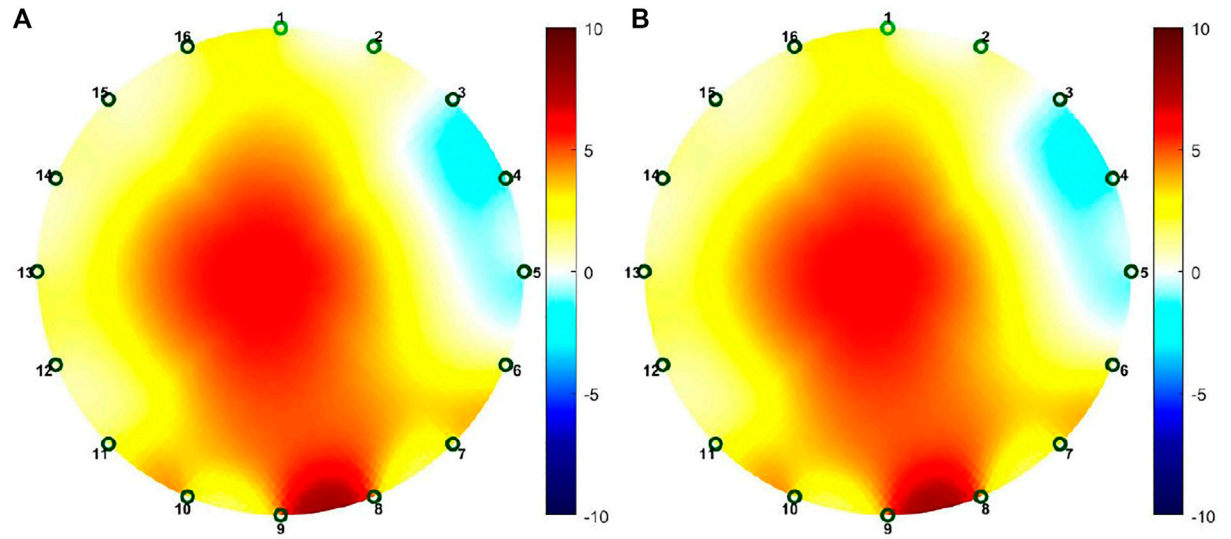

FIGURE 13 | (A) Image difference AX-f_c(ZX-ZM))-AM. The column average is used to correct the error. **(B)** Error Image AX-f_r(ZX-ZM))-AM. The row average is used to correct the error.

TABLE 1 | Quality factor of images obtained with multiplexing and error corrections.

Error correction method	Figure	QF
None	8	57
Method 1: element by element	9	83
Method 2: column-wise	10	67
Method 3: line-wise	11	67

in the future, for patients or healthy volunteers, will represent an enhancement for the calculations of EIT images. The confusing effect of multiplexers will be reduced by applying method 1 with factory-loaded compensating data. This article allows us to conclude that multiplexers are part of the design and that the error they introduce can be partially reduced.

DATA AVAILABILITY STATEMENT

The raw data supporting the conclusion of this article will be made available by the authors, without undue reservation.

AUTHOR CONTRIBUTIONS

MB, PS, JV, and MV designed IMPETOM-Clínico, defined EIDORS parameters, produced figures, made manual measurements, and wrote parts of the manuscript. IM contributed to the conceptualization of IMPETOM-Clínico, revised the manuscript, and checked the overall coherence of the research. AD supervised technical development of the laboratory work and contributed to figure generation, bibliographic research, and formatting of the manuscript. PB-F inspired the writing of this manuscript, supervised bibliographic research, corrected the manuscript, and gave general advice on electrical bioimpedance measurements. FS set the goals of research, supervised and gave general academic direction to the project as well as detailed article writing in English, and ensured logistics.

FUNDING

Funding was secured as part of regular teaching at the Universidad de la República and specifically came from the budget of Núcleo de Ingeniería Biomédica, Universidad de la República, Uruguay. Partial funding was obtained from Espacio Interdisciplinario, Universidad de la República and Comisión Sectorial de Investigación Científica (CSIC) de la Universidad de la República, Uruguay.

ACKNOWLEDGMENTS

The authors acknowledge the motivation of colleagues at an Electrical Bioimpedance Congress during which the decision to write the present article was made (CLABIO 2021 San Luis Potosí, México). The authors also acknowledge Agustín Mailing for contributions on the use of multiplexers and advice on software development.

REFERENCES

Adler, A., and Holder, D. (2021). *Electrical Impedance Tomography*. New York: CRC Press.

Adler, A., and Lionheart, W. R. B. (2006). Uses and Abuses of EIDORS: an Extensible Software Base for EIT. *Physiol. Meas.* 27, S25–S42. doi:10.1088/0967-3334/27/5/S03

Alfaro, N., Arregui, M., Martinucci, F., Santos, E., and Simini, F. (2015). *IMPETOM B - Inyección, adquisición y tratamiento inicial de señales para tomografía torácica por impedancia eléctrica en placa de pruebas Omap-L137*. Montevideo: Universidad de la República, Uruguay. [thesis]. [Montevideo].

Analog Devices Inc (1999). *A Technical Tutorial on Digital Signal Synthesis*. Available at: https://www.analog.com/en/education/education-library/technical-tutorial-dds.html (Accessed December 28, 2021).

Analog Devices Inc (2009). *MT-088 Tutorial "Analog Switches and Multiplexers Basics" Https:*. Available at://www.analog.com/media/en/training-seminars/tutorials/MT-088.pdf (Accessed February 17, 2022).

Bertemes-Filho, P. (2021). "Designing a Current Source," in *Bioimpedance and Spectroscopy*. Editors Annus. Paul and Mart. Min (Elsevier), 452. doi:10.1016/b978-0-12-818614-5.00003-5

Brown, B. (2009). Electrical Impedance Tomography (EIT): A Review. *J. Med. Eng. Tech.* 27 (3), 97–108. doi:10.1080/0309190021000059687

Calderón, A. P. (1980). "On an Inverse Boundary Value Problem" [in Seminar on Numerical Analysis and its Applications to Continuum Physics, *Math. Comput.* 52(186):553–559. doi:10.1090/s0025-5718-1989-0962208-x

Dräger AG (2020). *Dräger PulmoVista® 500*. Available at: https://www.draeger.com/es_csa/Home (Accessed December 28, 2021).

Ferreira, A., Rodríguez, A., Mazzara, P., and Simini, F. (2002). *IMPETOM-C: circuitos de generación de corrientes constantes de alta frecuencia y baja intensidad, y circuitos de medidas de voltajes destinados a la determinación de la bioimpedancia*. Montevideo: Universidad de la República, Uruguay. [thesis]. [Montevideo].

González, S., Liguori, A., and Simini, F. (2005). *IMPETOM Tomógrafo de Impedancia Eléctrica*. Montevideo: Universidad de la República, Uruguay. [thesis]. [Montevideo].

Grimnes, S., and Ørjan, G. M. (2015). *Bioimpedance and Bioelectricity Basics*. Oslo: Academic Press.

Harris, A. S., Zainuddin, N. F., Jamaludin, M. N., Asari, M. A., and PusppanathanMohd Latip, J. H. F. (2020). 16 by 3 Electrodes Electrical Impedance Tomography System Implementation on Cylindrical Phantom Design and Development. *IEEE EMBS Proc.*, 560–564. doi:10.1109/IECBES48179.2021.9398790

Hartman, R., Lobo, J., Ruétalo, M., and Simini, F. (2002). *IMPETOM-I Tomógrafo de impedancia eléctrica*. Montevideo: Universidad de la República, Uruguay. [thesis]. [Montevideo].

International Electrotechnical Commission (2020). IEC- 60479: Effects of Current on Human Beings and Livestock. Available at: https://www.iec.ch/(Accessed December 28, 2021).

International Electrotechnical Commission (2016). IEC-60990: Methods of Measurement of Touch Current and Protective Conductor Current. Available at: https://www.iec.ch/(Accessed December 28, 2021).

Jongschaap, H. C. N., Wytch, R., Hutchison, J. M. S., and Kulkarni, V. (1994). Electrical Impedance Tomography: a Review of Current Literature. *Eur. J. Radiol.* 18, 165–174. doi:10.1016/0720-048x(94)90329-8

Kao, T.-J., Saulnier, G. J., Isaacson, D., Szabo, T. L., and Newell, J. C. (2008). A Versatile High-Permittivity Phantom for EIT. *IEEE Trans. Biomed. Eng.* 55, 2601–2607. doi:10.1109/TBME.2008.2001287

Mohamadou, Y., Oh, T. I., Wi, H., Sohal, H., Farooq, A., Woo, E. J., et al. (2012). Performance Evaluation of Wideband Bio-Impedance Spectroscopy Using Constant Voltage Source and Constant Current Source. *Meas. Sci. Technol.* 23 (10), 105703. doi:10.1088/0957-0233/23/10/105703

Quinteros, W., Simini, F., and Gueido, D. (2007). *IMPETOM-48 Tomógrafo de Impedancia Eléctrica con tres hileras de electrodos*. Montevideo: Universidad de la República, Uruguay. [thesis]. [Montevideo].

Santos, E. (2014). *Alternativas de proyecto e implementación de circuitos y de programas de reconstrucción tendientes a un tomógrafo por impedancia eléctrica para la presentación compacta del estado edemático de cortes torácicos en tiempo real*. Montevideo: Universidad de la República, Uruguay. [master's thesis], [Montevideo].

Simini, F., Santos, E., and Arregui, M. (2018). *Electrical Impedance Tomography to Detect Trends in Pulmonary Oedema" in Bioimpedance in Biomedical Applications and Research*. Cham: Springer International Publishing, 45–64. doi:10.1007/978-3-319-74388-2_4

Swisstom (2015). *BB2 EIT*. Available at: http://www.swisstom.com/en/downloads_en (Accessed December 28, 2021).

Texas Instruments Inc. (2003). *Channel Analog Multiplexer/Demultiplexer, CD74HC406716*. Available at: https://www.ti.com/lit/gpn/CD74HC4067 (Accessed December 28, 2021).

Valentinuzzi, M. E., Rigaud, B., Morucci, J. P., Chauveau, N., and Felice, J. C. (1996). *Critical Reviews on Biomedical Engineering*. New York, NY: Begell House Inc, 599–654.

Wu, Yu., Hanzaee, Farnaz. Fahimi., Jiang, Dai., Bayford, Richard. H., and Demosthenous, Andreas. (2021). *Electrical Impedance Tomography for Biomedical Applications: Circuits and Systems Review*.

Zhu, J., Snowden, J. C., Verdejo, J., Chen, E., Zhang, P., Ghaednia, H., et al. (2021). "EIT-kit: An Electrical Impedance Tomography Toolkit for Health and Motion Sensing," in *The 34th Annual ACM Symposium on User Interface Software and Technology (UIST '21), October 10–14, 2021, Virtual Event* (USANew York, NY, USA: ACM), 14. doi:10.1145/3472749.3474758

Conflict of Interest: The authors declare that the research was conducted in the absence of any commercial or financial relationships that could be construed as a potential conflict of interest.

Publisher's Note: All claims expressed in this article are solely those of the authors and do not necessarily represent those of their affiliated organizations, or those of the publisher, the editors, and the reviewers. Any product that may be evaluated in this article, or claim that may be made by its manufacturer, is not guaranteed or endorsed by the publisher.

Copyright © 2022 Barreiro, Sánchez, Vera, Viera, Morales, Dell´Osa, Bertemes-Filho and Simini. This is an open-access article distributed under the terms of the Creative Commons Attribution License (CC BY). The use, distribution or reproduction in other forums is permitted, provided the original author(s) and the copyright owner(s) are credited and that the original publication in this journal is cited, in accordance with accepted academic practice. No use, distribution or reproduction is permitted which does not comply with these terms.